A Smart Cysteine-Activated and Heavy-Atom-Free Nano-Photosensitizer for Photodynamic Therapy to Treat Cancers

Shengze Su,[a] Xingcan Li,[a] Qian An,[a] Tao Liang,[d] Yanying Wang,[a] Hongping Deng,[c] Xiaoxing Xiong,[c] Wing-Leung Wong,[b,*] Huijuang Zhang,[a,*] Chunya Li,[a,c,*]

a. Key Laboratory of Catalysis and Energy Materials Chemistry of Ministry of Education & Hubei Key Laboratory of Catalysis and Materials Science & Key Laboratory of Analytical Chemistry of the State Ethnic Affairs Commission, South-Central Minzu University, Wuhan 430074, China.
b. State Key Laboratory of Chemical Biology and Drug Discovery, Department of Applied Biology and Chemical Technology, The Hong Kong Polytechnic University, Hung Hom, Kowloon, Hong Kong SAR 999077, China.
c. Renmin Hospital of Wuhan University, Wuhan University, Wuhan 430060, China.
d. Ministry of Education Key Laboratory for the Synthesis and Application of Organic Functional Molecules, Hubei University, Wuhan 430062, China.

* Corresponding author
E-mail (WLW): wing.leung.wong@polyu.edu.hk;
E-mail (HZ): zhjminda@mail.scuec.edu.cn;
E-mail (CL): lichychem@mail.scuec.edu.cn

Abstract:

A smart and heavy-atom-free photoinactive nano-photosensitizer capable of being activated by cysteine at the tumor site to generate highly photoactive nano-photosensitizer that showed strong NIR absorption and fluorescence with a good singlet oxygen quantum yield (16.8%) for photodynamic therapy was reported.

Cancer is a life-threatening disease. To develop effective and safe therapeutics for cancer treatment is critically important, particularly in improving the five-year survival rate of patients.[1] Compared to traditional treatments such as surgery, chemotherapy and radiotherapy, photodynamic therapy (PDT) provides some unique advantages including minimal invasiveness, low systemic toxicity and low drug resistance.[2] The formation of triple state in photosensitizer to empower $^1O_2$ and ROS production is a crucial process in PDT.[3] Currently, the most popular methods for design and construction of potent photosensitizers for PDT are to integrate heavy atoms such as Br, I, Ru and Os into organic fluorophores.[4, 5] However, this strategy causes a fast transition of T_1-S_0 that significantly reduces the lifetime of the triplet state of the photosensitizer.[6] It is thus not favourable for photosensitizers to produce $^1O_2$ and ROS to enhance photodynamic therapy efficiency. The physiological toxicity of heavy atoms is also a biosafety concern.[7] To tackle these challenges, to develop heavy-atom-free photosensitizers has become a new strategy.[8] Heavy-atom-free photosensitizers can be constructed by integrating electron donor and electron acceptor in an orthogonal geometry,[9] but the current development on this topic is still scarce. Moreover, to improve the target-specificity of heavy-atom-free photosensitizers for the imaging-guided antitumor therapy is important for clinical applications.

The reported heavy-atom-free photosensitizers are usually non-activatable.[7, 10] Most of them are excited by visible light, while those excited with near-infrared (NIR) light are rarely found.[11] Biothiols are typical biomarkers of human tumors and are involved in many physiological and pathological processes. Cysteine (Cys) concentration in normal human cells is found in the ranges of 30-200 μM and it is even higher in cancer cells.[12] In this regard, Cys could be employed as an *in vivo* activator to trigger tailored heavy-atom-free photoinactive photosensitizers to achieve a precise treatment with PDT. We thus attempted to develop new cysteine-activatable heavy-atom-free photosensitizers for PDT to treat human cancers.

We herein reported a new and smart NIR nano-photosensitizer that was heavy-atom-free, cysteine-activatable for PDT antitumor treatment. The proposed mechanism is shown in **Fig.**

1A. The NIR photosensitizer **OBT** can be formed *in situ* via Cys-activation from the nanoparticles integrated with **DNBT** (**DNBT NPs**). This smart intracellular Cys-triggerable NIR photosensitizer was structurally tailored with a BODIPY dye,[13] in which the *meso* position of the BODIPY scaffold was substituted by a 4-hydroxy-2,6-dimethylbenzene. Then, the hydroxy group was further modified with 2,4-dinitrobenzenesulfonate to act as a Cys-specific reaction site. **DNBT NPs** are designed to be photoinactive and the tagged 2,4-dinitrobenzenesulfonyl group is removed from **DNBT** upon reacted with Cys (**Fig. 1A**). Thus, a photoactive photosensitizer **OBT** is generated. Because the π-conjugated system of **OBT** is effectively extended, it shows a strong absorption band peaked at 700 nm (NIR region) and an emission band peaked at 740 nm, approximately. The resulting **OBT NPs** are highly active for PDT (**Fig. 1B**).

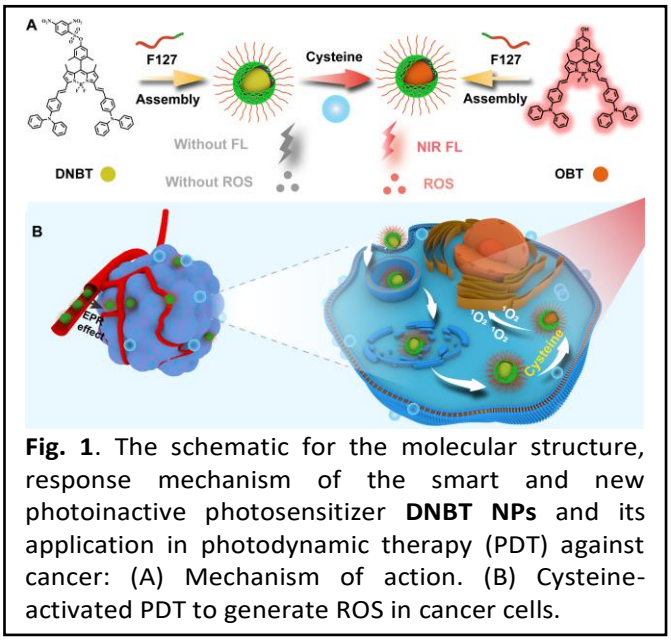

Fig. 1. The schematic for the molecular structure, response mechanism of the smart and new photoinactive photosensitizer **DNBT NPs** and its application in photodynamic therapy (PDT) against cancer: (A) Mechanism of action. (B) Cysteine-activated PDT to generate ROS in cancer cells.

The synthesis of photoinactive **DNBT NPs** was given in ESI.[14] The synthesis of **OMBDP** intermediate was shown in **Scheme S1**. The absorption and emission spectra of **OMBDP** were given in **Fig. S1**. The maximum absorption and emission wavelengths of the photosensitizer are 505 nm and 525 nm, approximately. The absorption characteristic of **OMBDP** is consistent with that of BODIPY.[15] Moreover, the fluorescence intensity of **OMBDP** in different solvents is found in the following order: toluene (Φ_F = 0.46), THF (Φ_F = 0.37) and methanol (Φ_F = 0.08), which are similar to the results reported previously.[16]

The ability of **OMBDP** to produce ROS in different solvents was investigated (**Fig. S2**). A 505 nm laser was selected as the excitation source and DPBF was used as an indicator to detect the formation of ROS.[17] From the DPBF degradation curves, the absorption peak of DPBF at 416 nm decreases with the increasing of irradiation time, indicating that **OMBDP** produces ROS under irradiation. Moreover, TMPO was used as a spin trapping agent for $^1O_2$. The irradiation of an **OMBDP** solution gives an induced EPR signal. The characteristic paramagnetic adducts (**Fig. S3**) are well-matched with $^1O_2$.[18] Also, **OMBDP** in toluene

provides better $^1O_2$ production than that in methanol due to solvent polarity, indicating that the $^1O_2$ production mechanism of the dye may follow SOCT-ISC mechanism.[11, 19]

As shown in **Fig. S4A**, **OBT**, modified from **OMBDP**, shows a maximum absorption peak at 679 nm, while **DNBT** shows a maximum absorption peak at 691 nm. After **DNBT** reacted with Cys, its maximum absorption wavelength was found the same as **OBT**. From **Fig. S4B**, **OBT** shows strong emission (λ_{max}=721 nm), while **DNBT** shows negligible fluorescence under the same condition. Notably, when **DNBT** reacts with Cys, it gives strong fluorescence peaked at 721 nm and the intensity is found almost the same as **OBT**. A mechanism for the reaction between **DNBT** and Cys is proposed as shown in **Fig. S5**. The relationship between the induced fluorescence intensity for **DNBT** reacting with Cys at different concentrations was investigated. From **Fig. S4 C-E**, the fluorescence intensity of **DNBT** was increased gradually with the increase of Cys concentration (0-100 μM) and showed a good linear response in the range of 0-50 μM. The selectivity of **DNBT** towards Cys was also investigated using glutamate, proline, glycine, lysine, ascorbic acid, hydrogen peroxide, histidine, thioglycolic acid, glutathione, cysteine, ·OH and Fe^{2+} ion as potential interferents.[20] The results (**Fig. S4F**) indicate that **DNBT** exhibits excellent selectivity towards Cys. Thus, the photoinactive **DNBT** is primarily triggered by Cys to form photoactive **OBT** *in-situ*.

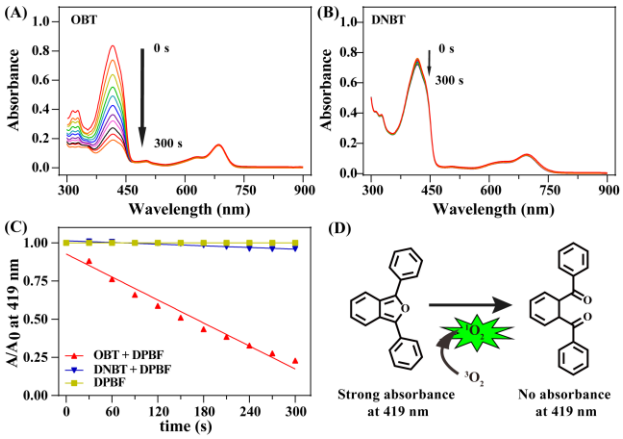

Fig. 2. The capability of the smart photosensitizer **OBT/DNBT** to generate ROS. UV-Vis absorption spectra of DPBF (100 μM) and **OBT** ((A), 2 μM) or **DNBT** ((B), 2 μM) under irradiation with 660 nm laser at different time (0 s, 30 s, 60 s, 90 s, 120 s, 150 s, 180 s, 210 s, 240 s, 270 s, and 300 s); (C) Normalized DPBF degradation induced by different compounds under 660 nm light irradiation; (D) Schematics for the response of DPBF towards $^1O_2$.

The ability of **OBT** and **DNBT** to generate $^1O_2$ in solution was investigated using DPBF as an indicator.[21] From **Fig. 2**, a fast degradation rate of DPBF was observed in a time-dependent manner in the **OBT**/DPBF system with an $^1O_2$ quantum yield (Φ_Δ) of 16.8% under a 660 nm laser irradiation. In the **DNBT**/DPBF system, no significant degradation of DPBF was found and $^1O_2$ quantum yield was 0.8% only. The results suggest that **DNBT** is photoinactive, while **OBT** is highly photoactive and produces $^1O_2$ in high yield to decompose DPBF in solution.

Both **DNBT NPs** and **OBT NPs** were synthesized using **DNBT** and **OBT** dyes to enable a potent and imaging-guided PDT *in vivo*.[22] The morphology of both nanoparticles was characterized with TEM and dynamic light scattering (DLS). As shown in **Fig. S6 A** and **C**, **OBT NPs** and **DNBT NPs** are spherical with an average size of 80-90 nm. From the DLS results (**Fig. S6 B** and **D**), the average hydrodynamic particle size is about 91 nm (**OBT NPs**) and 106 nm (**DNBT NPs**). Moreover, as shown in **Fig. S7 A** and **B**, the maximum absorption peak of **DNBT NPs** and **OBT NPs** are 718 nm and 696 nm, respectively. **OBT NPs** show intensive fluorescence (λ_{max}=746 nm), while **DNBT NPs** are not emissive.

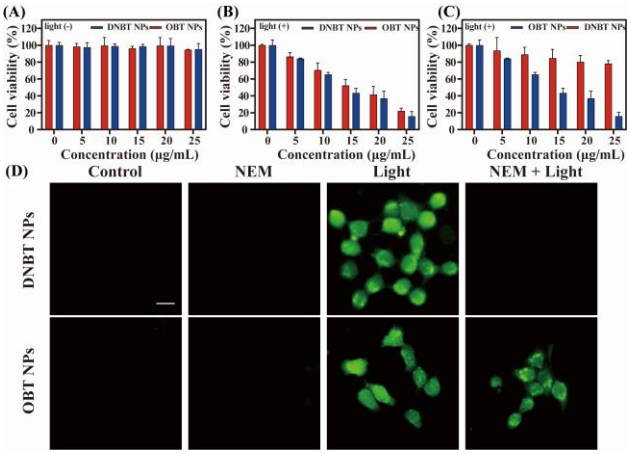

Fig. 3. The evaluation of the anticancer effect of **DNBT NPs** and **OBT NPs** in 4T1 cells. (Cell viability measures, each value represents the mean ± SD, n = 3). (A) Cell viability of 4T1 cells after being incubated with **DNBT NPs** or **OBT NPs** at different concentrations under dark conditions; (B) Cell viability of 4T1 cells after being incubated with **DNBT NPs** or **OBT NPs** at different concentrations under irradiation with a 660 nm laser (30 mW/cm^2, 20 min); (C) Cell viability of 4T1 cells after being incubated with NEM (0.5 mM) and then with **OBT NPs** and **DNBT NPs** at different concentrations under irradiation with a 660 nm laser (30 mW/cm^2, 20 min); (D) ROS analysis of 4T1 cells by DCFH-DA (20 mM, 30 min) with different treatments using confocal imaging. Scale bar: 20 μm.

To evaluate the ability of **DNBT NPs** and **OBT NPs** in generating ROS in PBS buffer, an indicator (ABDA) was utilized to detect ROS formed.[23] From **Fig. S8 A** and **B**, **OBT NPs** produce ROS under 660 nm laser irradiation, while **DNBT NPs** do not under the same condition. However, upon the addition of Cys to the solution of **DNBT NPs**, a remarkable ROS production was observed (**Fig. S8C**) and the ability to produce ROS was comparable to **OBT NPs** (**Fig. S8D**). The results provide further evidence that **DNBT NPs** are activated by Cys to generate photoactive **OBT NPs**, which are able to produce ROS effectively under a 660 nm laser irradiation.

To understand the anticancer effect of **DNBT NPs** and **OBT NPs**, they were incubated with breast cancer cells (4T1) and then monitored with confocal microscope for 0 to 360 min. From **Fig. S9**, the uptake of both nanoparticles by 4T1 cells is in a time-dependent manner, as indicated by an increased fluorescence intensity with increasing incubation time. Moreover, to study the PDT effects of **OBT NPs** and **DNBT NPs** against 4T1 cells, the toxicity under irradiation and under dark was examined. From **Fig. 3A**, under dark conditions, 4T1 cells incubated with **DNBT NPs** for 240 min or with **OBT NPs** for 180 min, the cell viability is

higher than 90%, even applying nanoparticles at 25 μg/mL. The results indicate that the nanoparticles possess high biocompatibility. Then, 4T1 cells were incubated with the nanoparticles under the same conditions and were irradiated with a 660 nm laser (30 mW/cm^2) for 20 min. From **Fig. 3B**, the inhibition of growth rate is 85%, indicating that both **DNBT NPs** and **OBT NPs** show high phototoxicity. The 4T1 cells treated with *N*-ethylmaleimide (NEM, 0.5 mM) were also incubated with **DNBT NPs** and then were irradiated with the laser for 20 min (30 mW/cm^2). From **Fig. 3C**, the ability of **DNBT NPs** for killing NEM-treated 4T1 cells was significantly reduced because NEM removed the Cys in the cells. In contrast, no obvious change was observed for **OBT NPs**. These results demonstrate that **DNBT NPs** are primarily activated by cellular Cys to form photoactive **OBT NPs** that show potent PDT effects.

DCFH-DA, a ROS fluorescent indicator, was used to further evaluate the mechanism of PDT mediated by **DNBT NPs** and **OBT NPs** in 4T1 cells.[24] From **Fig. 3D**, no green fluorescence response was detected in the treatment groups without 660 nm laser irradiation or NEM treatment.[1] In contrast, under irritation conditions, 4T1 cells treated with **DNBT NPs** and **OBT NPs** show bright green fluorescence, indicating the production of ROS. Moreover, no green fluorescence is detected for the NEM-treated group with **DNBT NPs** under a 660 nm laser irradiation, indicating that **DNBT NPs** in NEM-treated cells do not generate ROS. However, in the NEM-treated group with **OBT NPs** under a 660 nm laser irradiation, the intensive green fluorescence was observed clearly. These results indicate that NEM-treatment does not affect **OBT NPs** to produce ROS because **OBT NPs** are photoactive. Taken together, the cellular results observed in 4T1 cells under different conditions support that the photoinactive **DNBT NPs** after reacted with Cys in 4T1 cells are able to form photoactive **OBT NPs** that produce ROS under a 660 nm laser irradiation. The ROS generated *in cellulo* is presumably the key factor causing 4T1 cancer cell death.[25]

Live-dead cell staining for 4T1 cells treated under different conditions was performed using Calcein-AM/PI staining.[26] From **Fig. S10**, 4T1 cells incubated with **DNBT NPs** were irradiated by a 660 nm laser and showed intensive red fluorescence and few green fluorescence, indicating that most 4T1 cells were died. However, intensive green fluorescence was observed in the **DNBT NPs** treatment group without irradiation (dark condition), indicating that **DNBT NPs** possessed good biocompatibility and showed low toxicity against 4T1 cells. The thiol substances including Cys in 4T1 cells react with NEM effectively; however, the 4T1 cells treated with NEM alone do not show observable cell

death. Moreover, when co-incubating **DNBT NPs** with NEM-treated 4T1 cells, and then the cells were irradiated under a 660 nm laser, only green fluorescence (live cells) was observed, indicating no observable cell death. The results clearly support that intracellular Cys is an essential biomolecule to trigger and activate photoinactive **DNBT NPs** to generate PDT effects under irradiation. Nonetheless, some other cellular thiol biomolecules cannot be eliminated in the activation of **DNBT NPs** in cells. Furthermore, the induction of apoptosis in the 4T1 cells treated with **DNBT NPs** under light irradiation was verified with Annexin V-FITC and PI staining, and flow cytometry (**Fig. S11**, 73% apoptotic rate). The finding suggests that apoptosis may be the main death pathway of tumor cells in the treatment with PDT.

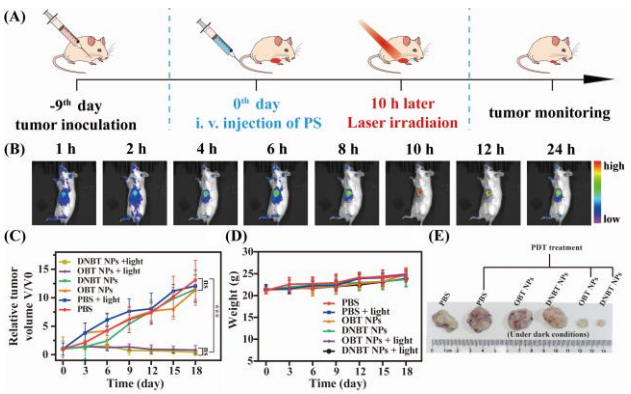

Fig. 4. The evaluation of *in vivo* efficacy of **DNBT NPs** and **OBT NPs** in PDT treatment. (A) Schematics for the *in vivo* treatment of the 4T1 tumor-bearing mouse; dose (200 μg/mL, 100 μL); laser irradiation (660 nm, 200 mW/cm^2, 20 min) post-injection (10 h). (B) *In vivo* fluorescence images of the tumor-bearing mouse after intravenous injection of **DNBT NPs** (200 μg/mL, 100 μL) acquired using a small animal *in vivo* imager; (C) The volume ratio of tumor after being treated under different conditions (each value represents the mean ± SD, n=3); (D) The variation of body weights of mice after being treated under different conditions; (E) The photo of tumors taken from mice with different treatment groups with/without PDT treatment.

To understand the *in vivo* efficacy of **DNBT NPs** and **OBT NPs** for PDT treatment, a tumor-bearing Balb/c mouse model was utilized for evaluation (**Fig. 4A**). The mice were randomly divided into 6 groups (PBS, PBS+light, **OBT NPs**, **DNBT NPs**, **OBT NPs**+light, and **DNBT NPs**+light). **DNBT NPs** dispersed in PBS buffer were injected into mice via tail vein. After 1 h, the fluorescence response was observable at the tumor site with an *in vivo* imaging system (**Fig. 4B**), indicating that the Cys in tumor tissues reacted with internalized **DNBT NPs** at the tumor site. As the photoinactive **DNBT NPs** is activated *in vivo* to give photoactive **OBT NPs** at the site, it is ready for PDT treatment. The fluorescence signal around tumor tissues was increased and the maximum intensive obtained was at 10 h after i.v. injection. This is an optimal post-injection time to start PDT treatment.

From **Fig. 4C**, the tumor volumes after PDT treatment were measured and recorded every 3-day for 18 days. On day 18, the tumor volume in the control, PBS and light irradiation groups, increased by about 12.5 times compared to their initial. Tumor volumes in the **DNBT NPs** and **OBT NPs** groups (under dark conditions) increased by about 11.2 times. Tumor

volumes in **DNBT NPs**+light group and **OBT NPs**+light group (irradiated at 660 nm, 200 mW/cm^2, for 20 min) were found comparable and significantly less than their initial, indicating that both **DNBT NPs** and **OBT NPs** effectively inhibited the growth of tumor with PDT. Moreover, body weights of mice show only slightly changes for all treatments (**Fig. 4D**).

Tumors were dissected from tumor-bearing mice under different treatment conditions for comparison. From **Fig. 4E** and **Fig. S12**, tumors isolated from **DNBT NPs**+light and **OBT NPs**+light groups were comparable and were significantly smaller than those from any other treatment groups. The *in vivo* results support that **DNBT NPs** show high efficacy for antitumor with PDT treatment. To further demonstrate the biocompatibility of **DNBT NPs** in the *in vivo* treatments, paraffin sections were performed for the major organs including heart, liver, spleen, lung and kidney of all mice and then stained with hematoxylin-eosin.[27] From **Fig. S13**, no observable physiological damage was found, indicating that there was no substantial systemic toxicity observed for using **DNBT NPs** in live mice.

In conclusion, a novel, smart and Cys-activatable photoinactive **DNBT NPs**, a heavy-atom-free and NIR photosensitizer, was successfully synthesized and demonstrated both *in cellulo* and *in vivo* for PDT anticancer applications The *in vivo* experiments using 4T1 tumor-bearing mice revealed that **DNBT NPs** showed high antitumor efficacy in PDT treatment and no substantial systemic toxicity associated with the *in vivo* use of **DNBT NPs** was observed in the major organs of mice. This study provides new insights into the design of smart, heavy-atom-free, Cys-triggerable NIR photosensitizers for antitumor therapy with high *in vivo* efficacy and low toxicity to normal tissues and organs.

Acknowledgments

This work was supported by National Natural Science Foundation of China (No. 22074160, 21874157, 22004133), Fundamental Research Funds for the Central Universities of South-Central Minzu University (No. CZZ22003), Open Project Funding of Ministry of Education Key Laboratory for the Synthesis and Application of Organic Functional Molecules, Hubei University (No. KLSAOFM2305), and Health and Medical Research Fund, Hong Kong SAR (No. 19200231).

Conflicts of interest

There are no conflicts to declare.

Notes and references

All animal experiments were approved by the Institutional Ethics Committee of South-Central Minzu University (No. 2022080A).

1. H. H. Han, H. M. Wang, P. Jangili, M. Li, L. Wu, Y. Zang, A. C. Sedgwick, J. Li, X. P. He, T. D. James and J. S. Kim, *Chem. Soc. Rev.*, 2023, **52**, 879-920.

2. X. B. Ma, M. C. Mao, J. Q. He, C. Liang and H. Y. Xie, *Chem. Soc. Rev.*, 2023, **52**, 6447-6496.
3. J. Miao, Y. Huo, G. Yao, Y. Feng, J. Weng, W. Zhao and W. Guo, *Angew. Chem. Int. Ed. Engl.*, 2022, **61**, e202201815.
4. K. X. Teng, L. Y. Niu and Q. Z. Yang, *J. Am. Chem. Soc.*, 2023, **145**, 4081-4087.
5. D. Hernandez-Castillo, R. E. P. Nau, M. A. Schmid, S. Tschierlei, S. Rau and L. Gonzalez, *Angew. Chem. Int. Ed. Engl.*, 2023, **62**, e202308803.
6. V. N. Nguyen, Y. X. Yan, J. Z. Zhao and J. Yoon, *Acc. Chem. Res.*, 2021, **54**, 207-220.
7. X. Z. Zhao, Q. C. Yao, S. Long, W. J. Chi, Y. X. Yang, D. Tan, X. G. Liu, H. Q. Huang, W. Sun, J. J. Du, J. L. Fan and X. J. Peng, *J. Am. Chem. Soc.*, 2021, **143**, 12345-12354.
8. X. Xiao, K. Y. Ye, M. Imran and J. Z. Zhao, *Applied Sciences*, 2022, **12**, 9933.
9. J. F. Miao, Y. Y. Huo, G. X. Yao, Y. Feng, J. J. Weng, W. Zhao and W. Guo, *Angew. Chem. Int. Ed. Engl.*, 2022, **61**, e202201815.
10. D. Xi, N. Xu, X. Xia, C. Shi, X. Li, D. Wang, S. Long, J. Fan, W. Sun and X. Peng, *Adv. Mater.*, 2022, **34**, 2106797.
11. Z. J. Wang and J. Z. Zhao, *Org. Lett.*, 2017, **19**, 4492-4495.
12. T. K. Chung, M. A. Funk and D. H. Baker, *The Journal of Nutrition*, 1990, **120**, 158-165.
13. A. Loudet and K. Burgess, *Chem. Rev.*, 2007, **107**, 4891-4932.
14. K. X. Teng, W. K. Chen, L. Y. Niu, W. H. Fang, G. Cui and Q. Z. Yang, *Angew. Chem. Int. Ed. Engl.*, 2021, **60**, 19912-19920.
15. J. N. Wang, J. L. Jin, Y. Geng, S. L. Sun, H. L. Xu, Y. H. Lu and Z. M. Su, *J. Comput. Chem.*, 2013, **34**, 566-575.
16. W. B. Hu, Y. H. Lin, X. F. Zhang, M. N. Feng, S. W. Zhao and J. Zhang, *Dyes Pigm.*, 2019, **164**, 139-147.
17. H. Kotani, K. Ohkubo and S. Fukuzumi, *Faraday Discuss.*, 2012, **155**, 89-102.
18. Z. X. Liu, Q. Wang, W. N. Qiu, Y. T. Lyu, Z. R. Zhu, X. L. Zhao and W. H. Zhu, *Chem. Sci.*, 2022, **13**, 3599-3608.
19. X. Xiao, W. Tian, M. Imran, H. M. Cao and J. Z. Zhao, *Chem. Soc. Rev.*, 2021, **50**, 9686-9714.
20. H. M. Guo, Y. Y. Jing, X. L. Yuan, S. M. Ji, J. H. Zhao, X. H. Li and Y. Y. Kan, *Org. Biomol. Chem.*, 2011, **9**, 3844-3853.
21. M. Zhao, Q. Zeng, X. Li, D. Xing and T. Zhang, *Nano Research*, 2022, **15** (1), 716-727.
22. M. Zhu, H. Zhang, G. Ran, D. N. Mangel, Y. Yao, R. Zhang, J. Tan, W. Zhang, J. Song, J. L. Sessler and J. L. Zhang, *J. Am. Chem. Soc.*, 2021, **143**, 7541-7552.
23. M. L. Liu, Y. C. Chen, Y. Guo, H. Yuan, T. X. Cui, S. K. Yao, S. X. Jin, H. H. Fan, C. J. Wang, R. Xie, W. J. He and Z. J. Guo, *Nat. Commun.*, 2022, **13**, 2179.
24. R. Wang, X. Xia, Y. J. Yang, X. Rong, T. Liu, Z. Su, X. L. Zeng, J. J. Du, J. L. Fan, W. Sun and X. J. Peng, *Adv. Healthc. Mater.*, 2022, **11**, 2102017.
25. L. K. B. Tam, L. Yu, R. C. H. Wong, W. P. Fong, D. K. P. Ng and P. C. Lo, *J. Med. Chem.*, 2021, **64**, 17455-17467.
26. Y. Yang, J. S. Huang, W. Wei, Q. Zeng, X. P. Li, D. Xing, B. Zhou and T. Zhang, *Nat. Commun.*, 2022, **13**, 3149.
27. S. Z. Su, L. Chai, Q. An, W. Hu, L. N. Wang, X. C. Li, H. J. Zhang and C. Y. Li, *Anal. Chem.*, 2022, **94**, 15146-15154.